Roberge-Weiss periodicity and singularity in a hadron resonance gas model with excluded volume effects

Riki Oshima[1,*], Hiroaki Kouno[1,†] and Kouji Kashiwa[2,‡]

[1]*Department of Physics, Saga University, Saga 840-8502, Japan*
[2]*Fukuoka Institute of Technology, Wajiro, Fukuoka 811-0295, Japan*

Quantum chromodynamics (QCD) with pure imaginary baryon number chemical potential $\mu = i\theta T$, where T is temperature and θ is a real number, has the Roberge-Weiss periodicity. We study the θ-dependence of the baryon number density and the pressure in the hadron resonance gas model with excluded volume effects of baryons. It is shown that the baryon number density and the pressure are smooth periodic functions of θ at low or high temperature. However, they have singular behavior at $\theta = (2k + 1)\pi$ where k is an integer, when $T \sim 211$ MeV. This temperature is consistent with the Roberge-Weiss transition temperature T_{RW} obtained by lattice QCD simulations. This singularity can be explained by the dual excluded volume effects in which the roles of pointlike and nonpointlike particles are exchanged each other in the ordinary excluded volume effects. It is also indicated that the excluded volume effect is visible just below T_{RW} and is directly detectable by the lattice QCD simulation at finite θ. We compare the results with the one obtained by the Polyakov-loop extended Nambu–Jona-Lasinio model.

I. INTRODUCTION

Determination of the phase diagram of quantum chromodynamics (QCD) is an important subject not only in nuclear and particle physics but also in cosmology and astrophysics; see, e.g., Ref. [1] and references therein. However, when the baryon number chemical potential is finite and real, the fist principle calculation, namely, the lattice QCD (LQCD) simulation, is not feasible due to the infamous sign problem; see Refs. [2,3] as an example. To circumvent the sign problem, several methods are proposed and investigated, although, at present, these methods are not complete and we do not have adequate information on the equation of state (EoS) at finite real baryon density.

One possible way to avoid the sign problem is to use the LQCD results with the imaginary baryon number chemical potential; see Refs. [4–8] as an example. When the baryon number chemical potential μ is pure imaginary, there is no sign problem. One can perform LQCD simulations at finite pure imaginary μ, and then make an analytic continuation from the quantities at imaginary μ to those at real μ.

Alternatively, one may determine the unknown parameters of an effective model of QCD using the LQCD results at finite imaginary μ. After determining the parameters, the model calculations can be performed at real μ [9].

It is known that the LQCD results at $\mu = 0$ are in good agreement with those obtained by the hadron resonance gas (HRG) model when temperature T is not so large. Usually, the ideal gas approximation is used for the calculations in the HRG model. However, it is expected that repulsive effects among baryons are important at high baryon number density. If the repulsion is absent, baryon matter is realized at a sufficiently large baryon density [10]. One of the traditional treatments for such repulsion is to consider excluded volume effects (EVE) among baryons [11–15]. EVE successfully prevents baryon matter from realizing at sufficiently large baryon density [11]; for the recent review, see, e.g., Ref. [16] and references therein. The availability of the HRG model with EVE may be checked by using the LQCD results at finite imaginary μ.

The grand canonical QCD partition function $Z(\theta)$ with pure imaginary quark chemical potential ($\mu_{\mathrm{q}} = \mu/3 = i\theta_{\mathrm{q}}T$) has the Roberge-Weiss (RW) periodicity [17] as

$$Z\left(\theta_{\mathrm{q}} + \frac{2\pi}{3}\right) = Z(\theta_{\mathrm{q}}), \qquad (1)$$

where T is the temperature and $\theta_{\mathrm{q}} \in \mathbb{R}$. This periodicity is the remnant of the $\mathbb{Z}_3$-symmetry of pure gluon theory. At low temperature, $Z(\theta_{\mathrm{q}})$ is expected to be a smooth function of θ_{q}. However, at high temperature above the RW temperature

---

*Contact author: 24804001@edu.cc.saga-u.ac.jp
†Contact author: kounoh@cc.saga-u.ac.jp
‡Contact author: kashiwa@fit.ac.jp

T_{RW}, it has a singularity at $\theta_q = (2k+1)\pi/3$ where $k \in \mathbb{Z}$. This singularity is called the RW transition. T_{RW} for $2+1$ flavor QCD is estimated as about 200 MeV by LQCD simulations [18–20].

In the HRG model with pure imaginary baryon number chemical potential $\mu = i\theta T$, the RW periodicity is trivial, since the model has a trivial periodicity

$$Z_{HRG}(\theta + 2\pi) = Z_{HRG}(\theta), \quad (2)$$

and $\theta := 3\theta_q$. In the case of the free hadron resonance gas, $Z_{HRG}(\theta)$ is a smooth function of θ at any temperature. However, it may have a singularity when interaction effects such as EVE are taken into account.

In this paper, we study the θ-dependence of the baryon number density and the pressure in the HRG model with EVE when the imaginary baryon number chemical potential is introduced, and analyze the mechanism of EVE at finite imaginary μ. It is shown that the baryon number density and the pressure have a singular behavior at $\theta = (2k+1)\pi$ when $T \sim 211$ MeV, while they are smooth functions of θ at lower and higher temperature. This result is consist with the previous result in Refs. [21,22] where the singularity of the HRG model with EVE was reported and its impacts were discussed, although our model is somewhat different from the previous ones. The singularity is understood by the dual EVE in which the roles of pointlike and nonpointlike particles are exchanged. The temperature $T \sim 211$ MeV is compatible with T_{RW} estimated by LQCD simulations. We also compare the results with the ones obtained by the Polyakov-loop extended Nambu–Jona-Lasinio (PNJL) model [23–28] in which the quark degree of freedom is contained.

This paper is organized as follows. In Sec. II, the RW periodicity and transition are briefly reviewed. In Sec. III, we show our formulation of the HRG model with EVE. The concept of dual EVE is also explained. In Sec. IV, numerical results are shown. Section V is devoted to the summary and discussions.

II. ROBERGE-WEISS PERIODICITY AND TRANSITION

The grand canonical partition function of QCD with imaginary $\mu = i\theta_q T$ is given by

$$Z(\theta_q) = \int \mathcal{D}\psi \mathcal{D}\bar{\psi} \mathcal{D}A_\mu e^{-S(\theta_q)}, \quad (3)$$

where

$$S(\theta_q) = \int_0^\beta d\tau \int_{-\infty}^\infty d^3x \mathcal{L}(\theta_q), \quad (4)$$

with

$$\mathcal{L}(\theta_q) = \bar{\psi}(\gamma_\mu D_\mu - m_0)\psi - \frac{1}{4}F_{\mu\nu}^2 - i\frac{\theta_q}{\beta}\bar{\psi}\gamma_4\psi, \quad (5)$$

here ψ, A_μ, D_μ, $F_{\mu\nu}$ and m_0 are the quark field, the gluon field, the covariant derivative, the field strength of gluon and the current quark mass matrix, respectively, and $\beta = 1/T$. The Euclidean notation is used in Eqs. (3)–(5).

To eliminate the θ_q-term from the action, we perform the following transformation of quark field:

$$\psi \mapsto \exp\left(i\frac{\tau\theta_q}{\beta}\right)\psi. \quad (6)$$

However, as a result, the antiperiodic temporal boundary condition ψ is changed as follows:

$$\psi(\mathbf{x}, \beta) = -\exp(i\theta_q)\psi(\mathbf{x}, 0). \quad (7)$$

This means that θ_q can be considered as the phase of the temporal boundary condition of quarks.

We perform another change of the quark and gluon fields

$$A_\mu \mapsto U(\mathbf{x}, \tau)A_\mu U^{-1}(\mathbf{x}, \tau) - \frac{i}{g}(\partial_\mu U(\mathbf{x}, \tau))U^{-1}(\mathbf{x}, \tau),$$

$$\psi \mapsto U(\mathbf{x}, \tau)\psi, \quad (8)$$

where g is a coupling constant, $U(\mathbf{x}, \tau)$ are elements of $SU(3)$ with the temporal boundary condition $U(\mathbf{x}, \beta) = z_3 U(\mathbf{x}, 0)$ and $z_3 = \exp(i2\pi k/3)$ is a $\mathbb{Z}_3$ element. The action $S(\theta)$ is invariant under this $\mathbb{Z}_3$ transformation but the quark boundary condition is changed as

$$\psi(\mathbf{x}, \beta) = -\exp\left[i\left(\theta_q + \frac{2\pi k}{3}\right)\right]\psi(\mathbf{x}, 0). \quad (9)$$

Hence, under the $\mathbb{Z}_3$ transformation, θ_q in $Z(\theta_q)$ is changed into $\theta_q + \frac{2\pi k}{3}$ and we obtain the RW periodicity (1) [17]. Dynamical quarks break the $\mathbb{Z}_3$-symmetry but the RW periodicity appears as a remnant of the $\mathbb{Z}_3$-symmetry.

At low temperature below the RW transition temperature T_{RW}, the baryon number density $n_Q/3$, where n_Q is the quark number density, is a smooth function of θ. However, at high temperature above T_{RW}, it is discontinuous at $\theta_q = (2k+1)\pi/3$ due to the degeneracy of the ground state. For illustrations, in Fig. 1, we show the θ_q-dependence of $n_Q/3$ obtained by the PNJL model [23–28] which is one of the most successful effective models of QCD. It is well known that the PNJL model can reproduce several important features of QCD at finite imaginary μ; for example, see Ref. [29] as a review. We also show the θ_q-dependence of pressure P_{PNJL} in Fig. 2. P_{PNJL} is a smooth function of θ_q when $T < T_{RW}$, while it has a cusp at $\theta_q = \pm\pi/3$ when $T > T_{RW}$. The RW periodicity and the RW transition are also confirmed by LQCD simulations and T_{RW} is estimated as 195–208 MeV for the $2+1$ flavor LQCD simulation [18–20].
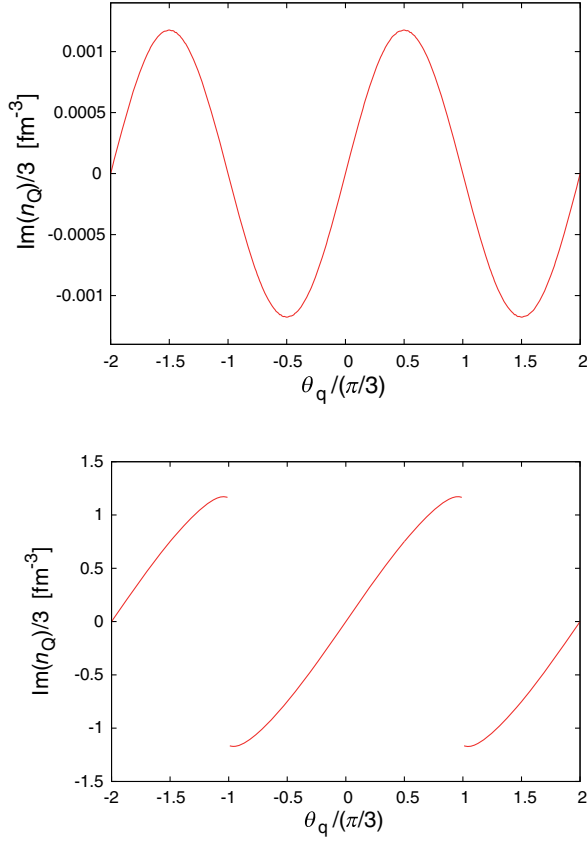
FIG. 1. The top (bottom) panel shows the θ_q-dependence of the imaginary part of the baryon number density $n_q/3$ when $T = 150$ MeV (250 MeV) in the PNJL model; see the Appendix for details of the model. Note that $T_{\rm RW} = 201$ MeV in this model. The discontinuities of n_q appear at $\theta_q = \pm\pi/3$ in the bottom panel.

FIG. 2. The top (bottom) panel shows the θ_q-dependence of the pressure $P_{\rm PNJL}$ when $T = 150$ MeV (250 MeV) in the PNJL model; see the cusps of $P_{\rm PNJL}$ appear at $\theta_q = \pm\pi/3$ in the bottom panel.

III. FORMULATION

In this section, we show the detailed formulation of the HRG model with EVE at finite T.

A. Excluded volume effects

Consider N nonpointlike particles in the system with volume V; see the top panel of Fig. 3. We regard that this system is equivalent to the system of N pointlike particle in the effective volume $V - vN$ where v is the volume of a nonpointlike particle [11]; see the bottom panel of Fig. 3. Hence, we obtain

$$n_{\rm p} = \frac{N}{V - vN} = \frac{n}{1 - vn}, \qquad (10)$$

where $n = N/V$ is the number density of nonpointlike particles and $n_{\rm p}$ is the one of N pointlike particles. Then, we obtain the number density n as
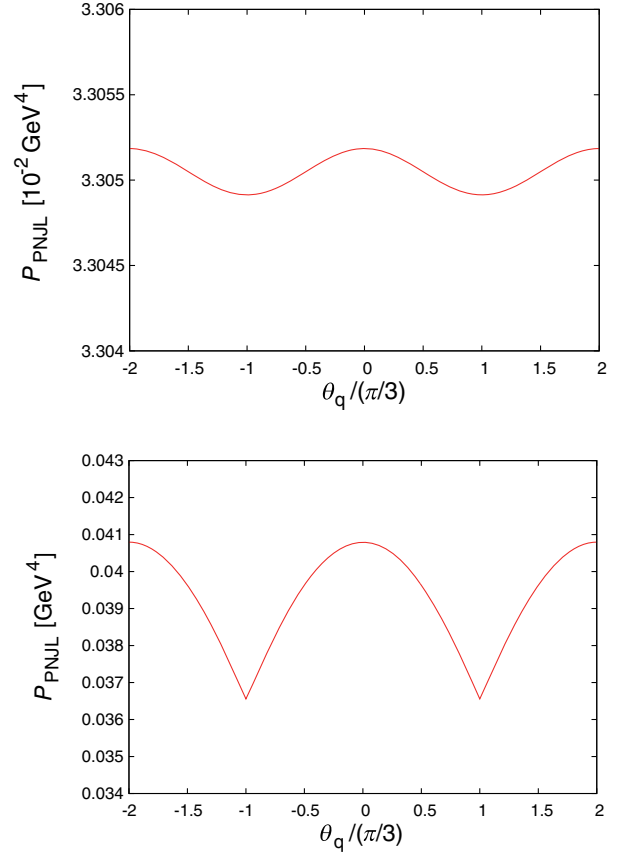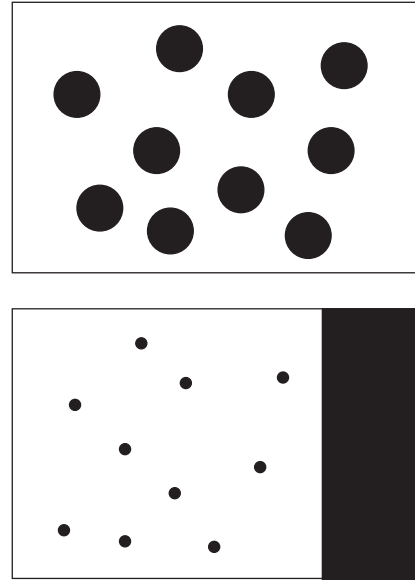

FIG. 3. The top and bottom panels show the schematic figure of the N nonpointlike particles in volume V and the N pointlike particles in the effective volume $V - vN$, respectively.

$$n = \frac{n_p}{1 + v n_p}. \tag{11}$$

Note that Eqs. (10) and (11) are valid only when the denominator is not zero. n can not exceed the upper bound $1/v$ when n_p is real and positive, and $n \to 1/v$ when $n_p \to \infty$.

If we replace v by $-v$, Eq. (10) is changed into

$$n_p = \frac{n}{1 + v n}. \tag{12}$$

Hence, $n_p \to 1/v$, when $n \to \infty$. In this paper, we call this effect "dual EVE." The dual EVE seems to be unnatural, since it is equivalent to EVE with a negative particle volume. However, later, we show that dual EVE actually occurs when the chemical potential is pure imaginary.

B. Hadron resonance gas model with excluded volume effects at finite temperature

Here, we consider the HRG model with EVE. At zero temperature, EVE is usually introduced for the baryon number N_B. However, at finite temperature, the number N_b of baryons and the number N_a of antibaryons do not vanish even if $N_B = N_b - N_a$ is zero. Hence, according to the next policy [12], we introduce EVE into the HRG model.

(1) Since EVE represents the effects of the repulsion forces among baryons, a baryon is affected by EVE of other baryons, but is not affected by EVE of antibaryons.

(2) Inversely, an antibaryon is affected by EVE of other antibaryons, but is not affected by EVE of baryons.

(3) Mesons are not affected by EVE. We treat the meson gas as a free gas of pointlike particles for simplicity.

Therefore, the baryon number density n_B of the system is given by

$$n_B(\mu) = n_b(\mu) - n_a(\mu), \tag{13}$$

with

$$n_b(\mu) = \frac{n_{bp}(\mu)}{1 + v n_{bp}(\mu)}, \tag{14}$$

$$n_a(\mu) = \frac{n_{ap}(\mu)}{1 + v n_{ap}(\mu)} = \frac{n_{bp}(-\mu)}{1 + v n_{bp}(-\mu)} = n_b(-\mu), \tag{15}$$

where n_b, n_a, n_{bp} and n_{ap} is the number densities of baryons, antibaryons, pointlike baryons and pointlike antibaryons, respectively. Here, we have assumed that v is the same for all baryons and antibaryons for simplicity. In numerical calculations, we set $v = 4\pi r_0^3/3$ with $r_0 = 0.8$ fm.

Note that n_B is an odd function of μ. Hence, when μ is a pure imaginary number, n_B is also a pure imaginary number, although n_b and n_a are complex numbers in general. The relations

$$\text{Re} n_b = \text{Re} n_a, \tag{16}$$

$$\text{Im} n_b = -\text{Im} n_a \tag{17}$$

with

$$\text{Re} n_b = \frac{\text{Re} n_{bp}(1 + v \text{Re} n_{bp}) + v(\text{Im} n_{bp})^2}{(1 + v \text{Re} n_{bp})^2 + v^2(\text{Im} n_{bp})^2},$$

$$\text{Im} n_b = \frac{i \text{Im} n_{bp}}{(1 + v \text{Re} n_{bp})^2 + v^2(\text{Im} n_{bp})^2},$$

$$\text{Re} n_a = \frac{\text{Re} n_{ap}(1 + v \text{Re} n_{ap}) + v(\text{Im} n_{ap})^2}{(1 + v \text{Re} n_{ap})^2 + v^2(\text{Im} n_{ap})^2},$$

$$\text{Im} n_a = \frac{i \text{Im} n_{ap}}{(1 + v \text{Re} n_{ap})^2 + v^2(\text{Im} n_{ap})^2}, \tag{18}$$

are realized since $\text{Re} n_{bp} = \text{Re} n_{ap}$ and $\text{Im} n_{bp} = -\text{Im} n_{ap}$, and thus the relation

$$n_B = 2i \text{Im} n_b = -2i \text{Im} n_a, \tag{19}$$

is manifested for Eq. (13).

When the free gas approximation is used, the concrete forms of n_{bp} and n_{ap} of ith baryon are given by

$$n_{bp,i} = \frac{g_{s,i}}{2\pi^2} \int_0^\infty dp \, p^2 \frac{1}{\exp\{\beta(\sqrt{p^2 + M_i^2} - \mu)\} + 1}, \tag{20}$$

$$n_{ap,i} = \frac{g_{s,i}}{2\pi^2} \int_0^\infty dp \, p^2 \frac{1}{\exp\{\beta(\sqrt{p^2 + M_i^2} + \mu)\} + 1}, \tag{21}$$

where $g_{s,i}$ and M_i are the spin degeneracy and the mass of the ith baryon, respectively. If we use the Boltzmann distribution instead of the Fermi distribution, Eqs. (20) and (21) are reduced to

$$n_{bp,i} = A_i(\cos\theta + i \sin\theta), \tag{22}$$

$$n_{ap,i} = A_i(\cos\theta - i \sin\theta), \tag{23}$$

with

$$A_i = \frac{g_{s,i}}{2\pi^2} \int_0^\infty dp \, p^2 e^{-\beta\sqrt{p^2 + M_i^2}}, \tag{24}$$

when μ is pure imaginary. Hence, the relation

$$\begin{aligned} \text{Re}[n_{bp}(\theta)] &= \text{Re}[n_{ap}(\theta)] \\ &= \text{Im}\left[n_{bp}\left(\theta + \frac{\pi}{2}\right)\right] \\ &= -\text{Im}\left[n_{ap}\left(\theta + \frac{\pi}{2}\right)\right], \end{aligned} \tag{25}$$

is satisfied.

In Ref. [12], the following simple form of pressure P_B of the baryon and antibaryon system with EVE was used;

$$P_B = \frac{P_{bp}}{1 + v n_{bp}} + \frac{P_{ap}}{1 + v n_{ap}}, \qquad (26)$$

where P_{bp} and P_{ap} are the pressures of pointlike baryons and antibaryons, respectively. However, this form of pressure does not satisfy the thermodynamical relation $\frac{\partial P_B}{\partial \mu} = n_B$ accurately. Then, we do not use the form (26). In this paper, the μ-dependence of baryon pressure P_B with EVE is given by

$$P_B(\mu) = P_b(\mu) + P_a(\mu) = P_b(\mu) + P_b(-\mu), \quad (27)$$

with

$$P_b(\mu) = \int_0^\mu d\mu' n_b(\mu') + P_b(0), \qquad (28)$$

where the initial conditions are given by

$$P_b(0) = \int_{-\infty}^0 d\mu' n_b(\mu'), \qquad (29)$$

respectively. In this formulation, the thermodynamical relation is automatically satisfied. Note that it is natural to assume $P_b(-\infty) = P_a(\infty) = 0$. In numerical calculations, we include all hadrons that are expected to be composed of a light quark only and are listed in the list of particle data [30].

In Refs. [21,22,31], the different formulation of EVE effects was used. In the formulation, the transcendental equations

$$P_b(T, \mu) = P_{bp}(T, \mu - bP_b), \qquad (30)$$

$$P_a(T, \mu) = P_{ap}(T, \mu - bP_a), \qquad (31)$$

are required, where $P_{bp}(P_{ap})$ is the pressure of the pointlike baryons (antibaryons) and b is the parameter which represents baryon (antibaryon) volume. In this paper, we call this formulation EVETC model, and call our formulation EVE model. In the next section, we compare the results of our formulation with those of EVETC.

IV. NUMERICAL RESULTS

In this section, we show our numerical results for the HRG model with EVE. First, we compare the results of the two formulations of EVE. Next, we show the θ-dependence of the baryon number density and the pressure, and discuss the effects of EVE below T_{RW}. We also show the same quantities above T_{RW}. Finally, we show the T-dependence of the pressure at $\theta = \pi$ and $\mu = 0 (\theta = 0)$.
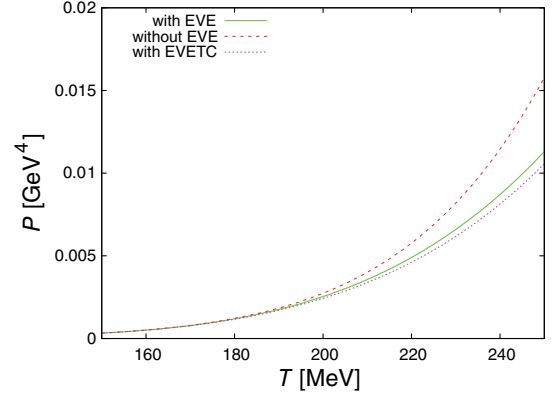

FIG. 4. The T-dependence of the pressure when $\mu = 0$ and $b = v = 4\pi r_0^3/3$. The solid, dashed, and dotted lines show the results obtained by the HRG models with EVE (P), without EVE (P_p), with EVETC, respectively.

A. Comparison of two formulation

In this subsection, we compare two formulations. Figure 4 shows the T-dependence of the pressure of the HRG model when $\mu = 0$ and $b = v = \frac{4\pi r_0^3}{3} = 2.14$ fm^3. We see that the exclude volume effects of EVE model is somewhat weaker than those of EVETC model, but the difference between two models is small. Figure 5 is similar to Fig. 4 but $b = 1.315$ fm^3 is used. We see that the result of EVE almost coincides with that of EVETC. In this case, it seems that the deference of the two models can be eliminated by retuning the parameter b. Figure 6 shows T-dependence of the pressure of HRG model when $\mu = 500$ MeV and $b = v = \frac{4\pi r_0^3}{3}$. We see that the difference between EVE and EVETC is small. Figure 7 is similar to Fig. 6 but $b = 1.315$ fm^3 is used. Again, we see that the result of EVE almost coincides with that of EVETC. Next, we examine the results at imaginary $\mu = i\theta T$. Figure 8 shows the T-dependence of the pressure of the HRG model
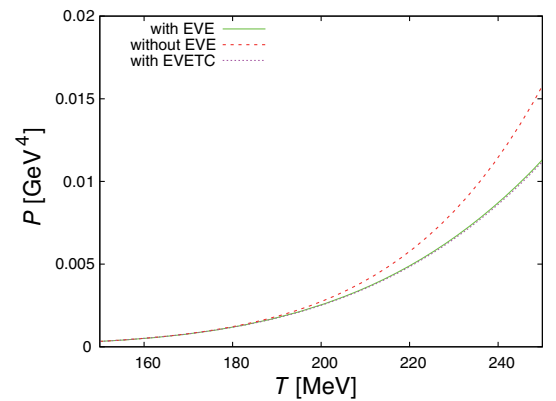

FIG. 5. The T-dependence of the pressure when $\mu = 0$, $v = 4\pi r_0^3/3$ and $b = 1.315$ fm^3. The solid, dashed, and dotted lines show the results obtained by the HRG models with EVE (P), without EVE (P_p), with EVETC, respectively.
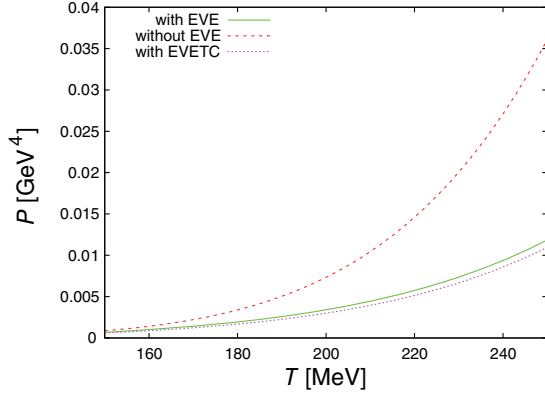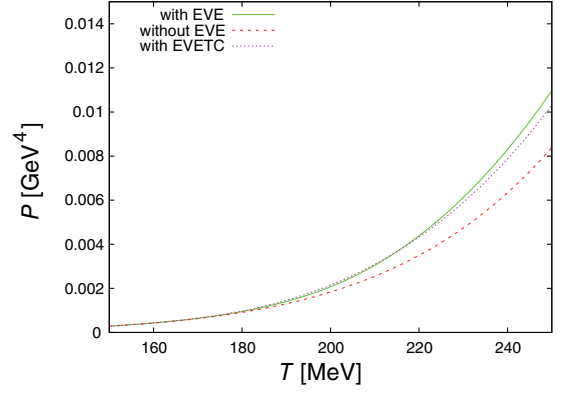
FIG. 6. The T-dependence of the pressure when $\mu = 500$ MeV and $b = v = 4\pi r_0^3/3$. The solid, dashed, and dotted lines show the results obtained by the HRG models with EVE (P), without EVE (P_p), with EVETC, respectively.

FIG. 7. The T-dependence of the pressure when $\mu = 500$ MeV, $v = 4\pi r_0^3/3$ and $b = 1.315$ fm^3. The solid, dashed, and dotted lines show the results obtained by the HRG models with EVE (P), without EVE (P_p), with EVETC, respectively.
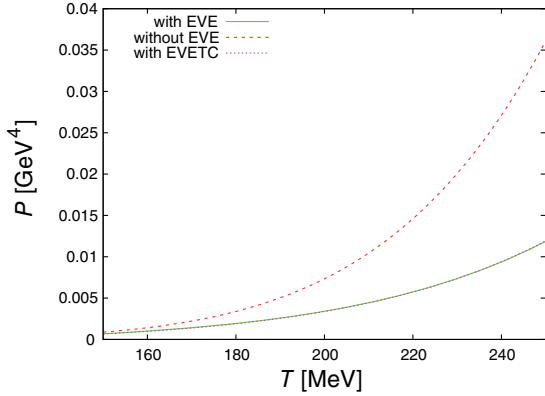

FIG. 8. The T-dependence of the pressure when $\theta = \frac{\pi}{2}$ and $b = v = 4\pi r_0^3/3$. The solid, dashed, and dotted lines show the results obtained by the HRG models with EVE (P), without EVE (P_p), with EVETC, respectively.
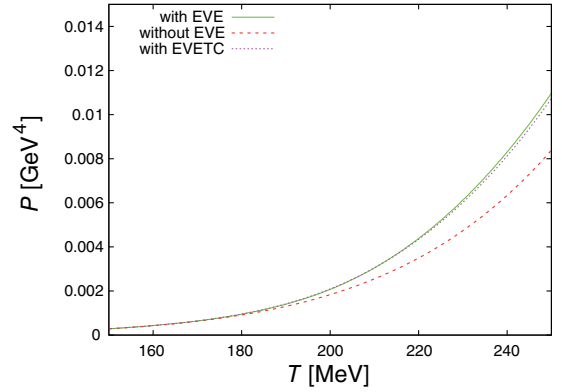

FIG. 9. The T-dependence of the pressure when $\theta = \frac{\pi}{2}$, $v = 4\pi r_0^3/3$ and $b = 1.315$ fm^3. The solid, dashed, and dotted lines show the results obtained by the HRG models with EVE (P), without EVE (P_p), with EVETC, respectively.

when $\theta = \frac{\pi}{2}$ and $b = v = \frac{4\pi r_0^3}{3}$. We see that the difference between EVE and EVETC is small. Figure 9 is similar to Fig. 8 but $b = 1.315$ fm^3 is used. The result of EVE almost coincides with that of EVETC. Comparison at the RW transition point will be shown in Sec. IV D.

B. Below T_{RW}

In this subsection, we show the θ-dependence of the baryon number density and the pressure, and discuss the effects of EVE below T_{RW}. Figure 10 shows the real and imaginary parts of n_b and n_{bp} as a function of θ when $T = 150$ MeV. We see that the real (imaginary) part is an even (odd) function of θ. We do not show the results of the antibaryon contributions explicitly, since conditions (16) and (17) are satisfied. As is expected, the relation $\mathrm{Re}[n_{bp}(\theta)] = \mathrm{Im}[n_{bp}(\theta + \frac{\pi}{2})]$ is approximately satisfied. The same relation is also approximately satisfied for n_b since EVE is negligible. Although we do not show all
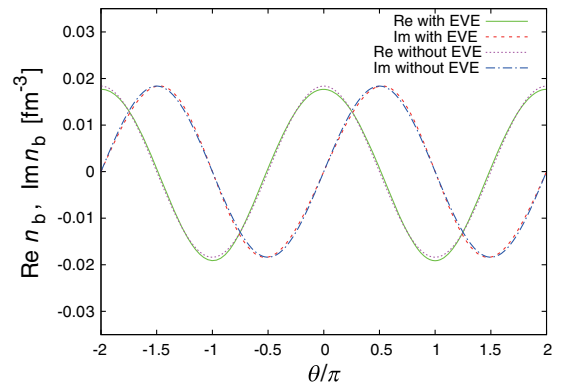

FIG. 10. The θ-dependence of the real and imaginary parts of number density of baryons when $T = 150$ MeV. The solid, dashed, dotted and dot-dashed lines show the results of $\mathrm{Re}n_b$, $\mathrm{Im}n_b$, $\mathrm{Re}n_{bp}$ and $\mathrm{Im}n_{bp}$, respectively.
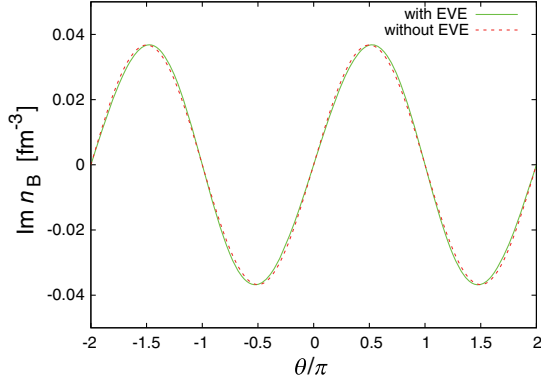
FIG. 11. The θ-dependence of imaginary part of baryon number density when $T = 150$ MeV. The solid and dashed lines show the results of n_{B} and n_{Bp}, respectively.

FIG. 13. The θ-dependence of the imaginary part of baryon number density when $T = 185$ MeV. The solid and dashed lines show the results of n_{B} and n_{Bp}, respectively.

results explicitly, the relation (25) is almost satisfied for n_{bp} and n_{ap} but is largely broken for n_{b} and n_{a}, when the temperature is large and EVE is not negligible. We also remark that, as in the case with $T = 150$ MeV, $\mathrm{Im}n_{\mathrm{bp}} = \mathrm{Im}n_{\mathrm{ap}} = 0$ and $\mathrm{Re}n_{\mathrm{bp}} = \mathrm{Re}n_{\mathrm{ap}} < 0$ are always satisfied at any temperature when $\theta = \pm\pi$. This is a very important property, as shown later. Figure 11 shows the imaginary part $\mathrm{Im}n_{\mathrm{B}}$ of baryon number density as a function of θ when $T = 150$ MeV. We see that EVE is negligible in this case.

Figure 12 shows the real and the imaginary parts of n_{b} as a function of θ when $T = 185$ MeV. We see that the equality $\mathrm{Re}[n_{\mathrm{b}}(\theta)] = \mathrm{Im}[n_{\mathrm{b}}(\theta + \frac{\pi}{2})]$ is broken largely by EVE. Figure 13 is the same as Fig. 11 but for $T = 185$ MeV. Note that the temperature $T = 185$ MeV is just below T_{RW} obtained by LQCD simulations. In this case, EVE is visible. These results indicate that the effects of EVE can be seen strongly at moderate T. Figure 14 shows the baryon pressure P_{B} as a function of θ; we do not show the meson pressure since it does not depend on θ in our model. Both P_{B} and P_{Bp} are smooth functions of θ. EVE is also visible in pressure.

C. Above T_{RW}

Figure 15 is the same as Fig. 11 but for $T = 210.8$ MeV. In this case, $\mathrm{Im}n_{\mathrm{B}}$ seems to be discontinuous at $\theta = \pm\pi$. The result resembles the one obtained by the PNJL model in the bottom panel of Fig. 1. However, different from the PNJL case, the height of the peak (the depth of the negative peak) increases as the minimal interval $\Delta\theta$ in the horizontal axis decreases in numerical calculation. It is very interesting that the temperature $T = 210.8$ MeV is slightly larger than T_{RW} obtained by LQCD simulations. As is mentioned above, $\mathrm{Im}n_{\mathrm{bp}} = \mathrm{Im}n_{\mathrm{ap}} = 0$ and $\mathrm{Re}n_{\mathrm{bp}} = \mathrm{Re}n_{\mathrm{ap}} < 0$ are always satisfied at any temperature when $\theta = \pm\pi$. Hence $\theta = \pm\pi$, the first and third ones of Eq. (18) reduce to

$$\mathrm{Re}n_{\mathrm{b}} = \frac{\mathrm{Re}n_{\mathrm{bp}}}{D(T)} = \mathrm{Re}n_{\mathrm{a}} = \frac{\mathrm{Re}n_{\mathrm{ap}}}{D(T)}, \qquad (32)$$

when

$$D(T) = 1 + v\mathrm{Re}n_{\mathrm{bp}} = 1 + v\mathrm{Re}n_{\mathrm{ap}}, \qquad (33)$$
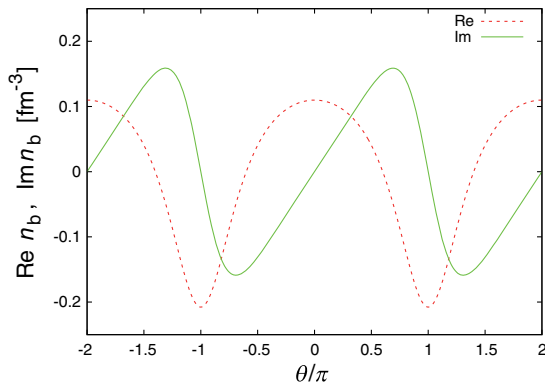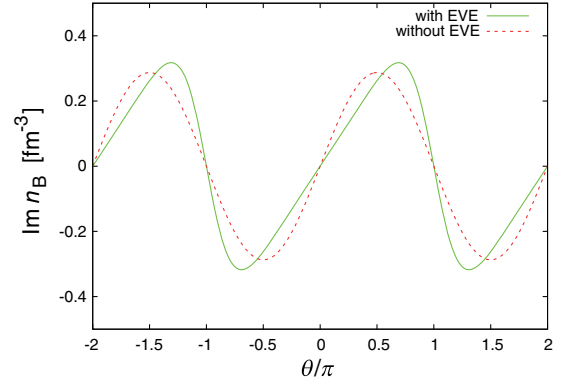

FIG. 12. The θ-dependence of the real and the imaginary part of number density n_{b} of baryons when $T = 185$ MeV. The dashed and solid lines show the results for the real and the imaginary part, respectively.
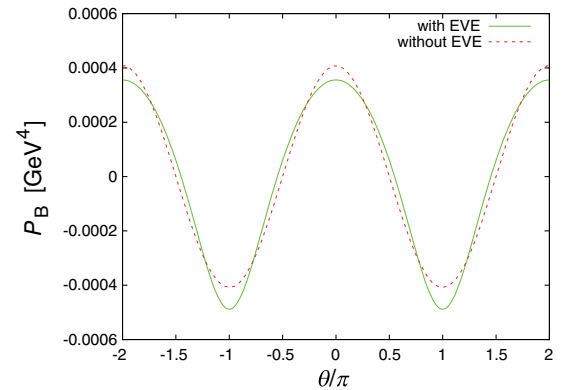

FIG. 14. The θ-dependence of the baryon pressure when $T = 185$ MeV. The solid and dashed lines show the results with EVE (P_{B}) and without EVE (P_{Bp}), respectively.
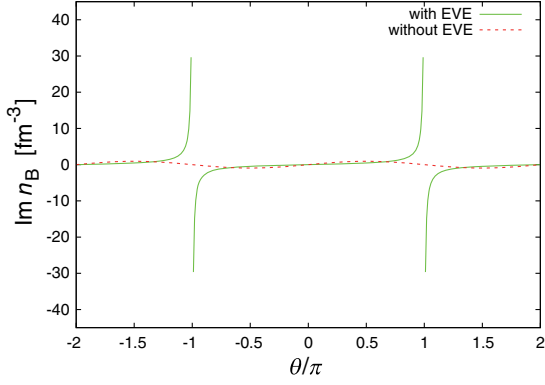
FIG. 15. The θ-dependence of the imaginary part of baryon number density when $T = 210.8$ MeV. The solid and dashed lines show the results of n_B and n_{Bp}, respectively.

FIG. 17. The T-dependence of n' at $\theta = \pi$.

does not vanish. Figure 16 shows $D(T)$ as a function of T when $\theta = \pi$. $D(T) = 0$ at $T = 210.8$ MeV. This means $\mathrm{Re}n_{bp} = \mathrm{Re}n_{ap} = -1/v$. The vanishing of $D(T)$ makes n_B singular at $T = 210.8$ MeV.

If we define $n' = -\mathrm{Re}n_b = -\mathrm{Re}n_a$ and $n'_p = -\mathrm{Re}n_{bp} = -\mathrm{Re}n_{ap} > 0$, Eq. (32) can be rewritten as

$$n' = \frac{n'_p}{1 - vn'_p}. \tag{34}$$

Hence, we obtain

$$n'_p = \frac{n'}{1 + vn'}. \tag{35}$$

This is nothing but the dual EVE (12). If $n' \to \infty$, $n'_p \to 1/v$. Figure 17 shows n' as a function of T when $\theta = \pi$. n' has a divergent behavior when $T \to 210.8$ MeV where $n'_p = 1/v$; note that the height of the peak (the depth of the negative peak) increases as the minimal interval ΔT in horizontal axis decreases in numerical calculation. In this paper, we call this situation "dual dense packing limit" of baryons. The dual dense packing of baryons causes the
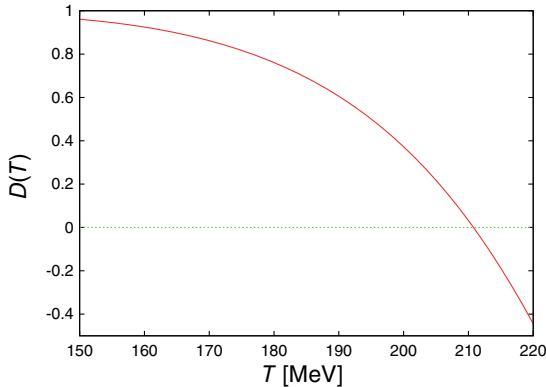
singularity; note that, although $\mathrm{Re}n_B$ always vanishes, the effects of $\mathrm{Re}n_{bp}$ and $\mathrm{Re}n_{ap}$ remain in other thermodynamic quantities such as $\mathrm{Im}n_B$ and pressure.

We also note that, when $n' < 0$, the interpretation of the dual EVE is not appropriate in (35). However, $n'_p \to 1/v$ is satisfied, when $n' \to -\infty$. Similarly, since $\mathrm{Re}n_{bp} < 0$, the interpretation of the EVE is not appropriate in (32), but $\mathrm{Re}n_b \to 1/v$ is satisfied when $\mathrm{Re}n_{bp} \to -\infty$. Hence, $1/v$ is the high temperature limit of $\mathrm{Re}n_b$ at $\theta = \pm\pi$.

When the Boltzmann distribution approximation is valid, we can define a μ-independent effective baryon radius as follows. In this approximation, $D(T)$ is reduced to $1 - v/v^*(T)$ where

$$v^*(T) = \frac{1}{A(T)}, \tag{36}$$

with

$$A(T) = \sum_i A_i. \tag{37}$$

Note that $A(T)$ is the amplitude of n_{bp} and n_{bp} when they oscillate as θ varies. Figure 18 shows an effective baryon radius $r^*(T) = [3v^*/(4\pi)]^{1/3}$ as a function of T. We see

FIG. 16. The T-dependence of $D(T)$ at $\theta = \pi$ (solid line). The dotted line shows the condition $D(T) = 0$.
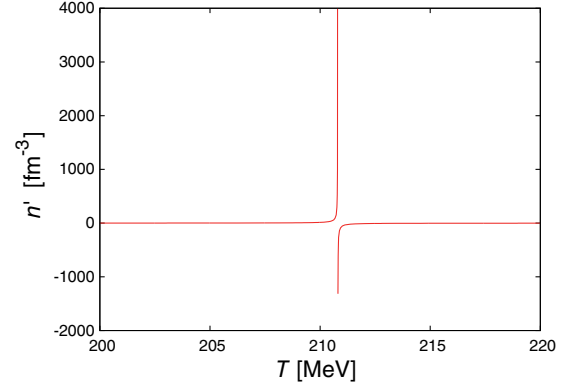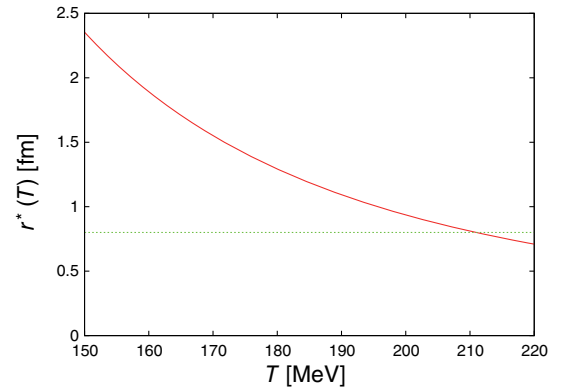

FIG. 18. The T-dependence of the effective baryon radius $r^*(T)$ at $\theta = \pi$ (solid line). The dotted line shows the condition $r^* = r_0 = 0.8$ fm.
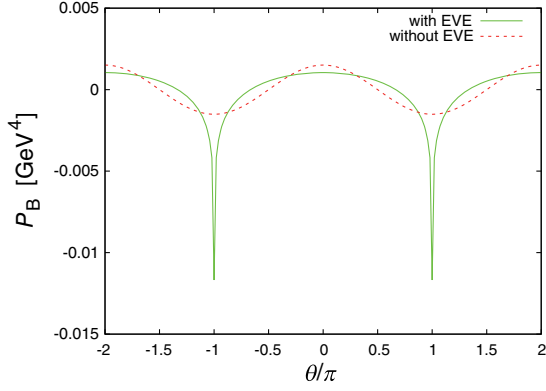
FIG. 19. The θ-dependence of the baryon pressure when $T = 210.8$ MeV. The solid and dashed lines show the results with EVE (P_B) and without EVE (P_{Bp}), respectively.

FIG. 21. The θ-dependence of the baryon pressure when $T = 250$ MeV. The solid and dashed lines show the results with EVE (P_B) and without EVE (P_{Bp}), respectively.

that $r^*(T) \sim r_0 = 0.8$ fm at $T \sim 211$ MeV. This means that the Boltzmann distribution approximation is valid in this case.

Figure 19 is the same as Fig. 14 but for $T = 210.8$ MeV. P_B has a cusp at $\theta = \pm\pi$, while P_{Bp} does not. The result of P_B resembles the one obtained by the PNJL model in the bottom panel of Fig. 2. However, different from the PNJL case, there is a tendency that the depth of the negative peak increases as the minimal interval $\Delta\theta$ in the horizontal axis decreases in numerical calculation. The cusp in P_B causes the discontinuity in Imn_B. Figure 20 is the same as Fig. 11 but for $T = 250$ MeV. In this case, Imn_b is a smooth function of θ as in the cases at low temperature. This feature is different from the PNJL result in Fig. 1 where the discontinuities appear when $T > T_{RW}$. Figure 21 is the same as Fig. 14 but for $T = 250$ MeV. Again, both P_B and P_{Bp} are smooth functions of θ. As is in the case with Imn_B, this feature is different from the PNJL result in Fig. 2 where the cusps appear when $T > T_{RW}$. The difference seems to be originated in the lack of quark degree of freedom in HRG model.
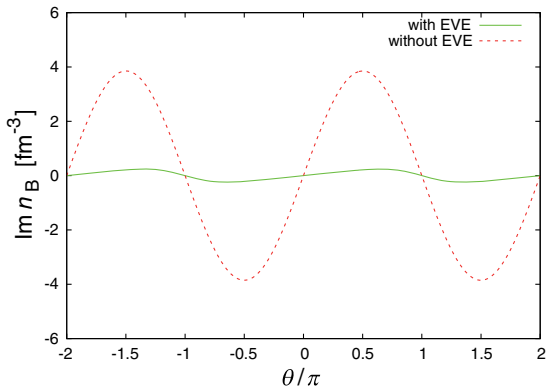
D. T-dependence of pressure

Figure 22 shows the hadron pressure as a function of T at $\theta = \pi$. Note that the meson contribution is included in the hadron pressure. The pressure P in the HRG model with EVE has a cusp at $T \sim 210.8$ MeV, while P_p in the HRG model without EVE is a smooth function of T; there is a tendency that the depth of the negative peak of P (P') increases as the minimal interval ΔT in the horizontal axis decreases in the numerical calculation. P_p increase as temperature increase when $T < 230$ MeV, but decreases $T > 230$ MeV. This is because the baryon contribution is negative at $\theta = \pi$ and the decrease of the negative baryon contribution overcomes the increase of the positive meson contribution when $T > 230$ MeV. On the contrary, P increases as T increases in the high temperature region, although it has a negative value in the intermediate temperature region.

In Fig. 22, the result obtained by the PNJL model is also shown. We have subtracted $P_{PNJL}(T = 0, \mu = 0) + B$ from

FIG. 20. The θ-dependence of the imaginary part of baryon number density when $T = 250$ MeV. The solid and dashed lines show the results of n_B and n_{Bp}, respectively.
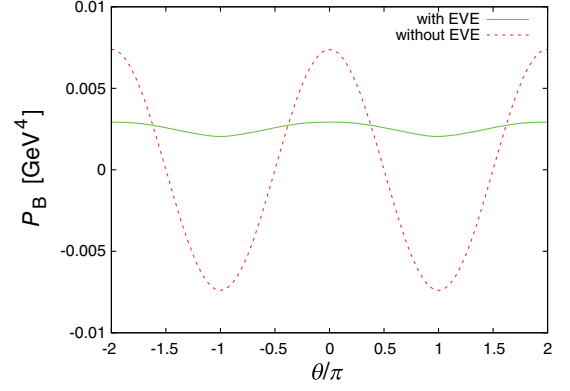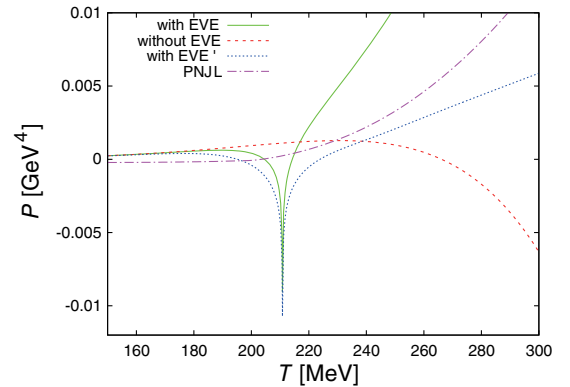

FIG. 22. The T-dependence of the pressure when $\theta = \pi$. The solid, dashed, dotted and dot-dashed lines show the results obtained by the HRG models with EVE (P), without EVE (P_p), with EVE plus meson gas suppression ($P' = P_B + P'_M$), and the PNJL model, respectively.

$P(T, \mu)$ where $B = (150 \text{ MeV})^4$ is the bag constant. P_{PNJL} is larger than P_p when $T > 229$ MeV, while it is smaller than P_p when $T < 229$ MeV. If we apply the Gibbs criteria to this case without EVE, the quark phase (hadron phase) is realized when $T > 229$ MeV ($T < 229$ MeV).

P_{PNJL} is larger than P in the region $T = 204$–214 MeV, while it is smaller in the other regions. If we apply the Gibbs criteria to this case with EVE, the quark phase is realized in the region $T = 204$–214 MeV and the hadron phase is realized otherwise. However, the HRG model with EVE may be invalid when $T > 210.8$ MeV, since it has a singularity. If this interpretation is appropriate, the quark phase is realized when $T > 204$ MeV.

It should be noted that the rapid increase of pressure of the HRG model with EVE in the high temperature region is caused by the rapid increase of meson contribution. In our model, the meson gas is treated as a free gas of pointlike particles. It is natural that the meson contribution is also suppressed in the high temperature region. For illustration, we assume the following simple suppression form of the meson pressure.

$$P'_M = P_M \exp\left[-(T/T^*)^{10}\right] \qquad (38)$$

We set $T^* = 210.8$ MeV. As is seen in Fig. 22, in this case, the hadron phase is realized in the low temperature and the quark phase is realized in the high temperature region ($T > 197$ MeV). The study of the mechanism of meson gas suppression is an important subject in the future.

Figure 23 shows T-dependence of the pressure of HRG model when $\theta = \pi$ and $b = v = \frac{4\pi r_0^3}{3} = 2.14$ fm^3. In the case of EVETC, we found the singular behavior at $T = 190.5$ MeV, but could not find the solution when $T > 190.5$ MeV. The temperature at which singularity

FIG. 24. The T-dependence of the pressure when $\theta = \pi$, $v = 4\pi r_0^3/3$ and $b = 1.315$ fm^3. The solid, dashed, and dotted lines show the results obtained by the HRG models with EVE (P), without EVE (P_p), with EVETC, respectively.

occurs is somewhat smaller in EVETC than EVE. Figure 24 is similar to Fig. 23 but $b = 1.315$ fm^3 is used. The difference of the singularity temperature is somewhat smaller than that in Fig. 23. As is in Fig. 23, we could not find the solution of EVETC when $T > 201$ MeV. It seems that the singularity temperature and the property of the pressure above the singularity temperature depend on the detail description of the model to some degree. However, qualitatively, the result of EVE is consistent with that of EVETC below the singularity temperature.

Figure 25 shows the same as Fig. 22 but for $\mu = 0$. We see that P_p and P are larger than P_{PNJL} at high temperature. Hence, if we apply the Gibbs criteria to these cases, the hadron phase is realized at high temperature. On the contrary, P' is smaller than P_{PNJL} at high temperature. In this case, the quark phase is realized at high temperature ($T > 216$ MeV). This fact confirms the importance of the meson pressure suppression.
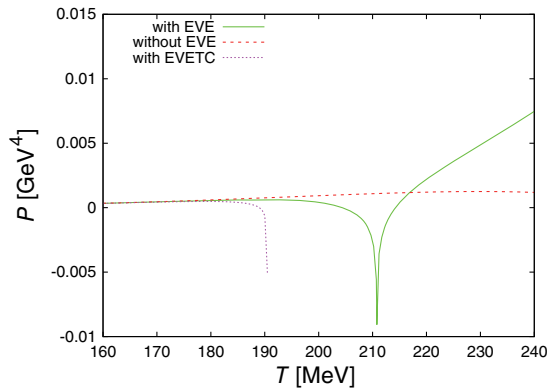

FIG. 23. The T-dependence of the pressure when $\theta = \pi$ and $b = v = 4\pi r_0^3/3$. The solid, dashed, and dotted lines show the results obtained by the HRG models with EVE (P), without EVE (P_p), with EVETC, respectively.
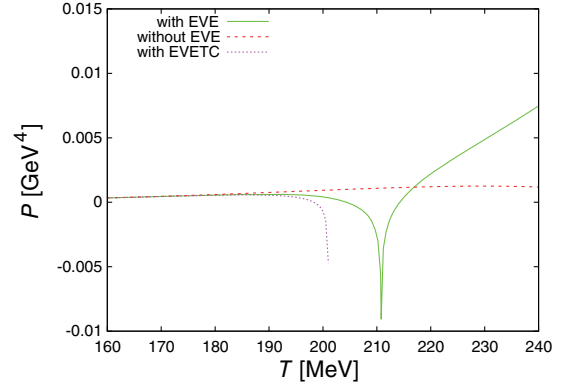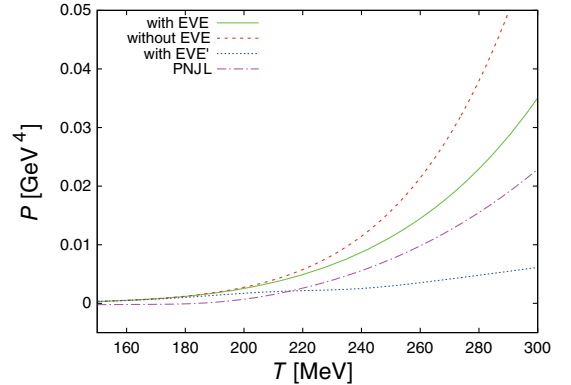

FIG. 25. The T-dependence of the hadron (PNJL) pressure when $\mu = 0$. The solid, dashed, dotted and dot-dashed lines show the results obtained by the HRG models with EVE (P), without EVE (P_p), with EVE plus meson gas suppression ($P' = P_B + P'_M$), and the PNJL model, respectively.

V. SUMMARY

In summary, in this paper, we have studied the baryon number chemical potential (μ) dependence of the baryon number density and pressure in the HRG model with excluded volume effects (EVE) when $\mu(= i\theta T)$ is pure imaginary. We compare the results with the ones obtained by the PNJL model in which the quark degree of freedom is contained.

In the HRG model, the Roberge-Weiss (RW) periodicity, which the QCD grand canonical partition function has, is trivial. At low temperature and high temperature, the θ-dependence of the baryon number density and the pressure are smooth functions of θ. However, they have a singular behavior at $\theta = (2k+1)\pi$ with $k \in \mathbb{Z}$ when $T \sim 211$ MeV which is consistent with the RW transition temperature $T_{\rm RW}$ obtained by lattice QCD (LQCD) simulations. This coincidence may reflect the simple fact that the inverse of the baryon radius $1/r_0$ is roughly estimated as 200 MeV. As T increases, the equality $\text{Re}(n_{\rm b}(\theta)) = \text{Im}(n_{\rm a}(\theta + \frac{\pi}{2}))$ is largely broken by EVE. This breaking of the equality seems to be important for the singular behavior at $T \sim 211$ MeV. It is very interesting that the singularity is well explained by the dual EVE in which the roles of pointlike and nonpointlike particles are exchanged with each other in EVE. In the picture of the dual EVE, the dual dense packing causes the singularity. At high temperature above $T \sim 211$ MeV, the singularity disappears. However, it is natural that the HRG model with EVE is valid only when the temperature is smaller than the temperature where the singularity appears. Since the dual EVE is equivalent to the EVE with a negative particle volume, it may be regarded as attractive force effects. It considerably lowers the pressure. Hadron matter with pressure of negative infinity cannot exist. Hadron matter is compressed and baryons are crushed by the strong attractive force at $\theta = (2k+1)\pi$ when $T \sim 211$ MeV. Hence, the introduction of the quark degree of freedom is necessary at higher temperature. The thermodynamic comparison between the HRG results and the PNJL results ensures this expectation.

It is also very interesting that EVE is visible just before $T_{\rm RW}$. EVE may be detectable by the LQCD simulation at imaginary μ [31]. If the function form of $\text{Im} n_{\rm B}$ deviates from the sine function, the EVE may be significant. In our calculations, we have treated v as a constant parameter. However, the T and/or the μ-dependence may be important; see, e.g., Ref. [32]. Such a dependence may be determined by the LQCD simulations.

ACKNOWLEDGMENTS

APPENDIX: PNJL MODEL

Thermodynamic potential density $\Omega_{\rm PNJL}$ in the three flavor PNJL model with the mean field approximation is given by [23–28]

$$\Omega_{\rm PNJL}(T,\mu_{\rm q}) = \mathcal{U}(T) + U_{\rm M} + \sum_{f=u,d,s} \Omega_f(T,\mu_{\rm q}), \quad (A1)$$

where

$$\Omega_f(T,\mu_{\rm q}) = -2\int \frac{d^3p}{(2\pi)^3}\left[3\sqrt{p^2+M_f^2} + T\log\left[f_f^-(p)f_f^+(p)\right]\right], \quad (A2)$$

with

$$f_f^-(p) = 1 + 3[\Phi + \Phi^* e^{-\beta E_f^-}]e^{-\beta E_f^-} + e^{-3\beta E_f^-},$$
$$f_f^+(p) = 1 + 3[\Phi^* + \Phi e^{-\beta E_f^+}]e^{-\beta E_f^+} + e^{-3\beta E_f^+}. \quad (A3)$$

where Φ, $\mathcal{U}$, $U_{\rm M}$ and M_f are the Polyakov loop, the Polyakov-loop potential, the mesonic potential and the effective mass of f-quark, respectively, and $E_f^\pm(p) = \sqrt{p^2+M_f^2} \pm \mu_{\rm q}$. The first term of the integrand in Eq. (A2) is a vacuum contribution. Note that the Polyakov-loop Φ and its conjugate Φ^* are complex, in general. The effective quark mass M_f is given by

$$M_f = m_f - 4G_{\rm S}\sigma_f + 2G_{\rm D}\sigma_f'\sigma_f'', \quad (A4)$$

with

$$f \neq f', \qquad f \neq f'', \qquad f' \neq f'', \quad (A5)$$

where m_f is the current quark mass of f-quark, $G_{\rm S}$ and $G_{\rm D}$ are coupling constants of four and six quarks interaction, and σ_f is the chiral condensate of f-quark, respectively. The mesonic part is given by

$$U_{\rm M} = 2G_{\rm S}(\sigma_u^2 + \sigma_d^2 + \sigma_s^2) - 4G_{\rm D}\sigma_u\sigma_d\sigma_s. \quad (A6)$$

According to Ref. [33], for model parameters, we set $m_{u,d} = 5.5$ MeV, $m_s = 140.7$ MeV, $G_{\rm S}\Lambda^2 = 1.835$, $G_{\rm D}\Lambda^5 = 12.36$ and $\Lambda = 602.3$ MeV. It should be noted that, to ensure the conformal limit at high temperature, we introduce a momentum cutoff Λ only in the vacuum part; the original PNJL model has a cutoff because it is a non-renormalizable model. For the Polyakov potential, we use the following form [27]:

$$\frac{\mathcal{U}(T; \Phi, \Phi^*)}{T^4} = \left[-\frac{a(T)}{2} \Phi^* \Phi + b(T) \log\{1 - 6\Phi^*\Phi \right.$$
$$\left. + 4(\Phi^3 + \Phi^{*3}) - 3(\Phi^*\Phi)^2\} \right] \qquad (A7)$$

where

$$a(T) = a_0 + a_1 \left(\frac{T_0}{T}\right) + a_2 \left(\frac{T_0}{T}\right)^2, \qquad (A8)$$

$$b(T) = b_3 \left(\frac{T_0}{T}\right)^3, \qquad (A9)$$

with modified coefficients [14,34]

$$a_0 = 2.457, \quad a_1 = -2.47, \quad a_2 = 15.2, \quad b_3 = -1.75. \quad (A10)$$

In numerical calculations, we set $T_0 = 220$ MeV so as to satisfy $T_{\mathrm{RW}} \sim 200$ MeV.

The pressure in the PNJL model is given by $P_{\mathrm{PNJL}} = -\Omega_{\mathrm{PNJL}}$. The number densities of f-quark and antiquark ($n_{\mathrm{q},f}$ and $n_{\mathrm{aq},f}$) are given by

$$n_{\mathrm{q}.f} = \frac{1}{\pi^2} \int_0^\infty dp \, p^2 \frac{g_f^-(p)}{f_f^-(p)}, \qquad (A11)$$

$$n_{\mathrm{aq}.f} = \frac{1}{\pi^2} \int_0^\infty dp \, p^2 \frac{g_f^+(p)}{f_f^+(p)}, \qquad (A12)$$

where

$$g_f^-(p) = 3\Phi e^{-\beta E_f^-} + 6\Phi^* e^{-2\beta E_f^-} + 3e^{-3\beta E_f^-}, \qquad (A13)$$

$$g_f^+(p) = 3\Phi^* e^{-\beta E_f^+} + 6\Phi e^{-2\beta E_f^+} + 3e^{-3\beta E_f^+}. \qquad (A14)$$

The solutions of $\sigma_f (f = u, d, s)$, Φ and Φ^* are determined so as to minimize Ω_{PNJL}.

[1] K. Fukushima and T. Hatsuda, Rep. Prog. Phys. **74**, 014001 (2011).

[2] P. de Forcrand, Proc. Sci. LAT2009 (**2009**) 010 [arXiv: 1005.0539].

[3] K. Nagata, Soryusironkenkyu **31**, 1 (2020), https://www2.yukawa.kyoto-u.ac.jp/~soken.editorial/author.html?author=%E6%B0%B8%E7%94%B0%20%E6%A1%82%E5%A4%AA%E9%83%8E; Prog. Part. Nucl. Phys. **127**, 103991 (2022).

[4] P. de Forcrand and O. Philipsen, Nucl. Phys. **B642**, 290 (2002).

[5] M. D'Elia and M.-P. Lombardo, Phys. Rev. D **67**, 014505 (2003).

[6] M. D'Elia and M.-P. Lombardo, Phys. Rev. D **70**, 074509 (2004).

[7] H.-S. Chen and X.-Q. Luo, Phys. Rev. D **72**, 034504 (2005).

[8] M. D'Elia and F. Sanfilippo, Phys. Rev. D **80**, 111501 (2009).

[9] Y. Sakai, K. Kashiwa, H. Kouno, M. Matsuzaki, and M. Yahiro, Phys. Rev. D **79**, 096001 (2009).

[10] J. Cleymans, R. V. Gavai, and E. Suhonen, Phys. Rep. **130**, 217 (1986).

[11] J. Cleymans, K. Redlich, H. Satz, and E. Suhonen, Z. Phys. C **33**, 151 (1986).

[12] H. Kouno and F. Takagi, Z. Phys. C **42**, 209 (1989).

[13] D. H. Rischke, M. I. Gorenstein, H. Stoecker, and W. Greiner, Z. Phys. C **51**, 485 (1991).

[14] A. Miyahara, M. Ishii, H. Kouno, and M. Yahiro, Phys. Rev. D **101**, 076011 (2020).

[15] K. S. Jeong, L. McLerran, and S. Sen, Phys. Rev. C **101**, 035201 (2020).

[16] Y. Fujimoto, K. Fukushima, Y. Hidaka, A. Hiraguchi, and K. Iida, Phys. Lett. B **835**, 137524 (2022).

[17] A. Roberge and N. Weiss, Nucl. Phys. **B275**, 734 (1986).

[18] C. Bonati, M. D'Elia, M. Mariti, M. Mesiti, F. Negro, and F. Sanfilippo, Phys. Rev. D **93**, 074504 (2016).

[19] F. Cuteri, J. Goswami, F. Karsch, A. Lahiri, M. Neumann, O. Philipsen, C. Schmidt, and A. Sciarra, Phys. Rev. D **106**, 014510 (2022).

[20] C. Bonati, E. Calore, M. D'Elia, M. Mesiti, F. Negro, F. Sanfilippo, S. F. Schifano, G. Silvi, and R. Tripiccione, Phys. Rev. D **99**, 014502 (2019).

[21] K. Taradiy, A. Motornenko, V. Vovchenko, M. I. Gorenstein, and H. Stoecker, Phys. Rev. C **100**, 065202 (2019).

[22] O. Savchuk, V. Vovchenko, R. V. Poberezhnyuk, M. I. Gorenstein, and H. Stoecker, Phys. Rev. C **101**, 035205 (2020).

[23] K. Fukushima, Phys. Lett. B **591**, 277 (2004).

[24] C. Ratti, M. A. Thaler, and W. Weise, Phys. Rev. D **73**, 014019 (2006).

[25] S. K. Ghosh, T. K. Mukherjee, M. G. Mustafa, and R. Ray, Phys. Rev. D **73**, 114007 (2006).

[26] E. Megias, E. Ruiz Arriola, and L. L. Salcedo, Phys. Rev. D **74**, 065005 (2006).

[27] S. Rößner, C. Ratti, and W. Weise, Phys. Rev. D **75**, 034007 (2007).

[28] Y. Sakai, T. Sasaki, H. Kouno, and M. Yahiro, Phys. Rev. D **82**, 076003 (2010).

[29] K. Kashiwa, Symmetry **11**, 562 (2019).

[30] R. L. Workman et al. (Particle Data Group), Prog. Theor. Exp. Phys. **2022**, 083C01 (2022).

[31] V. Vovchenko, A. Pasztor, Z. Fodor, S. D. Katz, and H. Stoecker, Phys. Lett. B **775**, 71 (2017).

[32] H. Kouno and K. Kashiwa, Phys. Rev. D **109**, 054007 (2024).

[33] P. Rehberg, S. P. Klevansky, and J. Hufner, Phys. Rev. C **53**, 410 (1996).

[34] A. Miyahara, M. Ishii, H. Kouno, and M. Yahiro, Int. J. Mod. Phys. A **32**, 1750205 (2017).